Removal of Cationic Dye – Methylene Blue- from Aqueous Solution by Adsorption on Fly Ash-based Geopolymer

M. EL Alouani, S. Alehyen*, M. EL Achouri, M. Taibi

Mohammed V University in Rabat,
Laboratoire de Physico-chimie des Matériaux Inorganiques et Organiques (LPCMIO), Ecole Normale Supérieure BP :
5118. Takaddoum -Rabat-Morocco

Abstract

The aim of this work is to investigate the workability of removing methylene blue (MB) from aqueous solution using fly ash based geopolymer powder (FAG). The FAG was formulated by mixing fly ash (FA) and alkaline activator in an appropriate ratio. The FA and FAG were characterized by physical and chemical techniques, such as X-ray fluorescence spectroscopy, X-ray diffraction (XRD), Fourier Transform Infrared (FTIR) and Scanning Electron Microscopy (SEM). To optimize the process of removing MB onto FAG, different parameters were studied such as, the effect of pH, initial dye concentration, adsorbent dosage, contact time and temperature. The results show that the maximum removal efficiency of MB was found in the basic environment. Isotherm studies showed that the adsorption of MB using FAG followed Langmuir model and the maximum adsorption capacity of MB is about 37.04 mg/g. Kinetic studies show that the adsorption process follows the pseudo second-order kinetic. The thermodynamic study indicated that the adsorption was favorable, endothermic and spontaneous.

1. Introduction

Dyes are important compound commonly used in various industries such as textile, paper, leather and plastic manufacture [1]. The discharge of dye-containing effluent without proper treatment into water bodies causes both environmental and public health risks [2]. Among the textile dyes most used in industry, methylene blue (MB) or basic blue 9. It is a water-soluble cationic dye and can reveal very harmful effects on living things such as difficulties in breathing, vomiting, diarrhea, nausea and several negative impacts on the aquatic environment [3]. Therefore it is very important to confirm the water quality, since even just 1.0 mg/L of dye concentration in drinking water can impart a significant color, making it unfit for human consumption [4]. Therefore, it is necessary to reduce dyes concentration in wastewater.

Nowadays, various technologies are available for the degradation of pollutants from wastewaters, such as biological treatment [5], biochemical methods [6], membrane separation [7], ion-echange [8], ultrafiltration [9], electrochemical processes [10], coagulation/flocculation [11], adsorption [12-14] and other processes. In recent years, many scientists are interested in the synthesis of the new adsorbents for removing the organic and inorganic pollutants from wastewaters by the adsorption method. Adsorption has some advantage when compared aforementioned conventional methods in terms the simplicity of utilization, effectiveness, low cost, ect. However, different adsorbents have been investigated for the adsorption of different types of pollutants from water and wastewater, such as Fly ash[15-19], chitosan [20], silica[21],natural phosphate[22], clay minerals [23], activated carbon [24], metakaolin-based geopolymer [25] and fly ash based geopolymer[26,27]. The goal is to find a desirable adsorption material for degradation of hazardous substances from wastewaters. The geopolymeric adsorbents have attracted considerable scientific attention in the field of environmental remediation.

The term geopolymer was coined by Davidovits 1978 [28, 29]. The geopolymer or known as inorganic polymer is a new class of synthetic alumina-silicate materials that involves a chemical reaction between alumina-silicate oxides and alkali metal silicate solutions under highly alkaline conditions [30]. Corresponding to different Si/Al ratios, the geopolymers are composed of network structures of polysialate (-O-Si-O-Al-O-), polysialate siloxo (-O-Si-O-Al-O-Si-O-), and polysialate disiloxo (O-Si-O-Al-O-Si-O-Si-O-) [31,32].

In this situation, FAG is a typical example of an abundant material that has been widely used in wastewater treatment. Various authors [33-35] have mentioned the importance of the synthesis the FAG to remove the hazardous substances from wastewater.

The aim objectives of present study were to synthesis the FAG and to examine its effectiveness in the removal of MB from aqueous solution by adsorption. In this context, the effect of various parameters such as adsorbent ratio, pH, contact time, initial dyes concentration and temperature on the adsorption efficiency of MB was evaluated. The adsorption kinetic was analyzed using the pseudo-first order, pseudo-second order and the intraparticle diffusion model. The experimental equilibrium data were examined using Langmuir, Freundlich, Temkin and Dubinin–Radushkevich. The thermodynamics of was also determined.

2. Materials and methods

2.1. Synthesis of FAG

FAG was prepared using FA and alkaline solution. The FA sample used in this study was from thermal coal plant of Jorf lasfar in Morocco. The alkaline activator was synthesized using sodium silicate powder (Honeywell Riedel-de Haën®, Germany; 18 wt.% Na_2O, 63 wt.% SiO_2, 18wt.% loss on ignition) and sodium hydroxide (ACS AR Analytical Reagent Grade Pellets). The alkali silicate activator was elaborated by mixing the NaOH and Na_2SiO_3 solution at the mass ration 2.5 and the concentration of NaOH solution was 12 M. The FAG was formulated by mixing fly ash with an alkali silicate solution, with solid-to-liquid ratio of 2.5. The role of the sodium silicate is to support sufficient Si^{4+} and improve the formation of geopolymer precursors [36]. The paste was then poured in a cylindrical container for curing at a temperature of 60°C for 24 h, the FAG was obtained treating in ambient temperature for 3 days. The sample was crushed, sieved through sieve to obtain lower fractions (<200μm). Before, the adsorption test. The composition and microstructure of samples were characterized by XRD, FTIR, FX, SEM and TEM microscopy.

2.2. Dye cationic

In the present work, the dye used in all the experiments was MB. The chemical formula and some other specific characteristics of cationic dye are presented in Table 1. The stock solution of MB was prepared of 1000 mg/L in distilled water. The MB used in the work was the analytical grade on (Aldrich Chemistry, Germany).

Table 1: Physicochemical characteristics of used dye

Name	λ_{max} (nm)	Molar mass (g/mol)	Molecular structure
Methylene Blue $C_{16}H_{18}ClN_3S$	664	319,852	
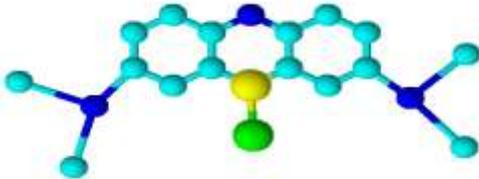
2.3. Characterization

The fly ach (FA) and fly ash based geopolymer (FAG) were characterized by many physico-chemical methods: The chemical compositions were obtained by X-ray fluorescence using a spectrometer dispersion wavelength - Type Axios. X-ray diffraction (XRD) patterns of the samples were obtained using a Xpert Pro model diffractometer equipped with a monochromatic with a source operating Cu-Kα (1.54060 Å). The Fourier transform infrared (FTIR) spectra of the samples were recorded by the KBr pellet technique on a VERTEX 70 FTIR spectrometer, in the spectral range of 4000–400 cm^{-1} with 4 cm^{-1} resolution. Image of FA was

characterized by a detector type (SUTW-Sapphire, Resolution: 230.89, Lsec: 111).The morphology and structure of the FA and FAG were characterized by a scanning electron microscope (SEM) analysis and Transmission electron microscopy (TEM).

2.4. Batch adsorption tests

Adsorption experiments were performed using 250 mL Erlenmeyer flasks containing desired weight of adsorbent, 100 mL of MB solution and the mixture was stirred gently with speed of 250 rpm. The effects of pH medium, adsorbent mass, contact time, initial concentration of MB and temperature are presented in Table 2.

Table 2: Summary of adsorption experiments conditions

Investigated parameter	Temperature (°C)	pH	Geopolymer dosage (g)	Contact time (min)	Initial concentration (mg/L)
Geopolymer dosage (g)	25	5	0.05 0.1 0.15 0.2 0.25 0.3	120	40
Contact time (min)	25	5	0.1	0 30 60 90 120 150 180 220	20, 30, 40
pH	25	2.5 4.5 5 6.3 9.8 11.2	0.1	120	40
Temperature (°C)	20 50 70	5	0.1	120	40
Initial conc. (mg/L)	25	5	0.1	120	5 10 20 40 60

The pH of solution was adjusted using 0.1M NaOH and 0.1M HCl solutions and measured using a Meter Lab, pH M 210 meter. Batch adsorption tests were used to determine the % Removal and the quantity of dye adsorbed of MB onto FAG. After each completed adsorption test, the sample was separated by centrifuge at 2500 rpm for 10 min to separate the solid phase from the liquid phase and the concentration of dye was determined from its UV-Vis absorbance characteristic with the calibration method. The concentration of the solution before and after adsorption was measured using A JASCO V-630 UV/VIS spectrophotometer.

The efficiency of Methylene blue (MB), % Removal, was calculated using:

$$\% \operatorname{Re}moval = \frac{(C_i - C_t)}{C_i} \times 100 \qquad (1)$$

Where C_i is the initial concentration (mg.L^{-1}), and C_t is the concentration (mg.L^{-1}) at any time t.

Adsorption capacity at time t, q_t (mg.g^{-1}), was obtained as follows:

$$q_t = \frac{(C_i - C_t)}{m} V \qquad (2)$$

Where V (L) is the volume of the solution and m (g) is the mass of FA based geopolymer.
Adsorption capacity at equilibrium, q_e (mg.g^{-1}), was calculated using:

$$q_e = \frac{(C_i - C_e)}{m} V \qquad (3)$$

Where C_e (mg.L^{-1}) is the equilibrium concentration.

3. Results and discussion
3.1. Characterization of FA and FAG
3.1.1. X-ray diffraction (XRD) analysis and X-ray fluorescence (XRF) analyses
The chemical composition of FA and FAG in this study is shown in Table 3. It is apparent by XRF that FA mainly consists of SiO_2, Al_2O_3, Fe_2O_3 and CaO. The sum of the SiO_2, Al_2O_3 and Fe_2O_3 is above 70 wt% of the sample mass is characteristic of Class-F fly ash [37]. After modification by activator solution (geopolymerization), it was found for FAG with a Si/Al ratio lower than 2.4 that the geopolymer had a poly-sialate-siloxo (PSS) (-Si-O-Al-O-Si-O-) [38,39].

The XRD patterns of FA and FAG are given in Fig.1. The results of XRD analysis of the FA and FAG indicated that quartz (SiO_2) and mullite ($3Al_2O_3.2SiO_2$) were the chief crystalline phase. After geopolymerization process, the shift of peak towards lower frequencies is due to the formation of new product and the peak between 22° and 28° (2 Theta) indicates the presence of amorphous aluminosilicate gel [40]. The result indicates that the presence the alkali activator leads to the formation of amorphous phases.

Table 3: Chemical compositions of FA and FAG

Major oxides (wt %)	FA	FAG	Major elements (wt %)	FA	FAG
SiO_2	52.5	39.6	O	50.6	45.7
Al_2O_3	30.2	14.7	Na	0.534	18.8
Fe_2O_3	2.94	3.31	Si	24.6	18.5
MgO	1.23	0.66	Al	16	7.76
CaO	0.822	0.682	Fe	2.06	2.31
Na_2O	0.719	25.4	K	1.73	1.33
K_2O	2.08	1.6	Ti	0.62	0.579
TiO_2	1.03	0.97	Ca	0.587	0.487
P_2O_5	0.203	0.124	Mg	0.744	0.398
SO_3	0.719	0.453	S	0.315	0.181
Loss on ignition	7.12	11.8	Cu	0.315	0.11
SiO_2/Al_2O_3	1.73	2.7	Si/Al	1.54	**2.4**

3.1.2. Fourier Transform Infrared Spectroscopy (FTIR) Analysis
An infrared analysis was performed on FA and FAG. IR spectrum shown in Fig.2 and all the band assignments are listed in Table 4. IR spectrum showed signification change in position of peaks. The bands appeared in the regions of 1622 cm^{-1} and 3441cm^{-1} that were attributed to bending vibrations (H–O–H) and stretching vibrations O–H. The bands appeared in the regions of 457 and 734 cm^{-1} are due to the vibration mode Si-O-Al and Si–O–Si, respectively. Which confirm the presence of mullite and quartz [41]. After geopolymerization process, the band existing at 1458 cm^{-1} assigned to the stretching vibrations of O–C–O bond occurred in all alkali activated FA samples implying to the presence of the sodium bicarbonate. The shift recorded, to 1075 cm^{-1} (Fig.2.a) and 1005 cm^{-1} (Fig.2.b), is indicative of formation of network in a geopolymer structure [40]. This observation is also supported by the XRD results showing the presence of amorphous phase and the formation of new reaction product.
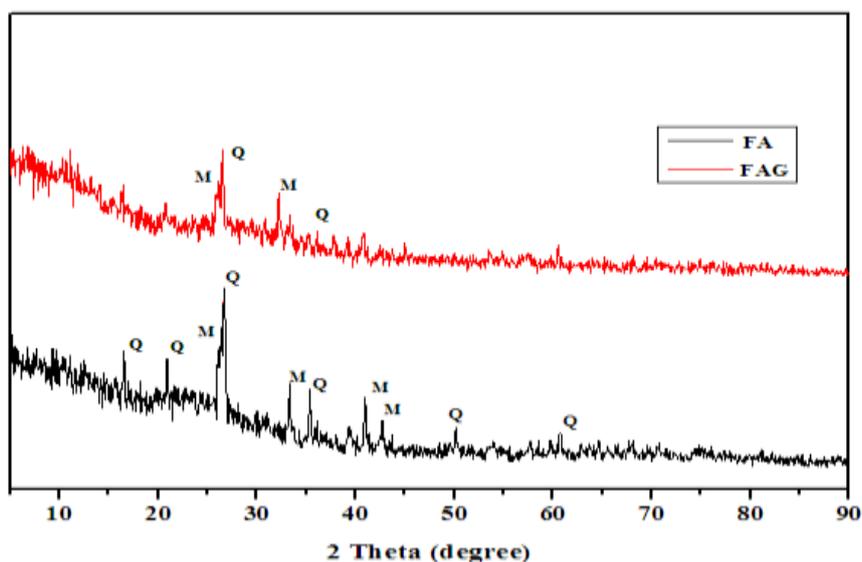
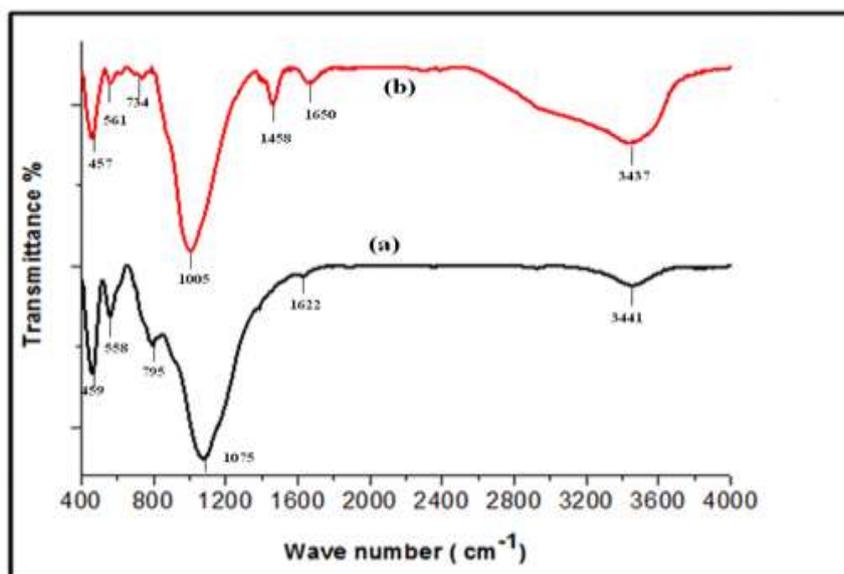**Figure 1:** XRD patterns of FA and FAG (Q: Quartz; M: Mullite)

Figure 2: FTIR specta of FA (a) and FAG (b)

Table 4: FTIR spectrum analysis

Materials	Bands (cm^{-1})	Assignments	References
FA	3441, 1622	Stretching and deformation of OH. H– O–H groups from the water molecules	[42-44]
	1075	stretching vibration of groups (Si-O)	[45]
	795	Stretching vibration Al-O	[46]
	558	Bending vibration Si-O-Al	[47]
	459	Bending vibration Si-O-Si	[49]
FAG	3437, 1650	Stretching and deformation of OH and H–O–H groups from the water molecules	[48-49]
	1458	stretching vibration of O-C-O	[50]
	1005	stretching vibration of groups (Si-O)	[45]
	734	Bending vibration Si–O–Si	[51]
	561	Bending vibration Si-O-Al	[47]
	457	Al-O/ Si-O bendling vibration	[51]

3.1.3. Scanning electron microscope (SEM/EDX) analysis

Scanning electron microscopy (SEM) was used to observe the surface texture of FA and FAG. Fig.3 described a change in the structure of the FA after the polymerization by activating the FA with an alkaline solution. The absence of the spherical particles in geopolymer material synthesized from FA and alkali solution indicates high conversion on FA to crystalline geopolymer. It is clear that the new microstructure of geopolymer played an important role on its adsorption capacity. The FA was analyzed via EDX to quantify the surface chemical elements, as shown in Fig.4.a.b, the major portion of the FA is composed of Si and Al compounds. In addition to TEB analysis, image of FA is shown in Fig.4.c, as can be seen, the particle shapes of the FA were generally spherical and smooth surfaces.
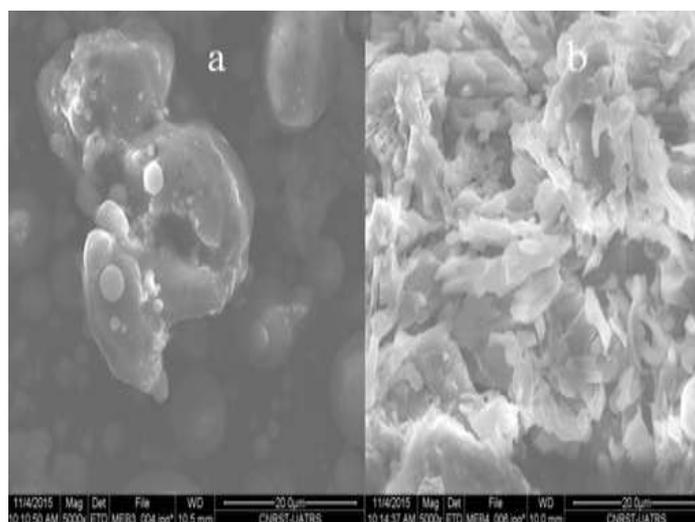

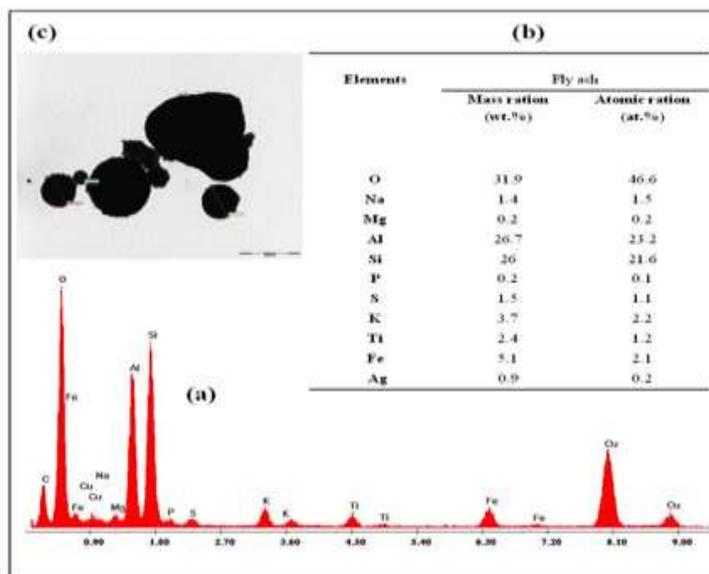**Figure 3:** SEM micrograph of FA (a) and FAG (b)

Figure 4: EDX micrograph (a), the surface chemical composition (b) and TEB image of FA (c)

3.2. Adsorption the dye onto materials

3.2.1. Effect of adsorbent ratio

Adsorbent ratio is a very important parameter in the determination of adsorption capacity [52] and the effect of quantity of adsorbent in optimization of quantity plays a vital role in adsorption process of MB using FAG. The results for adsorption of MB onto geopolymer are showed in Fig.5. The results revealed that as the percentage of adsorption increase by increasing the quantity of adsorbent in range 0.05 and 0.15 g. After 0.15 g, the maximum removal level is for MB was observed at 0.15 g.
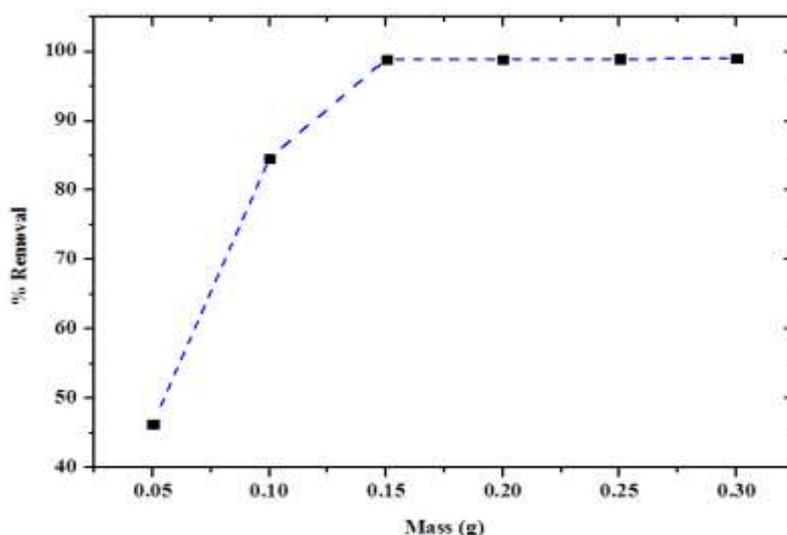
Figure 5: Effect of adsorbent dose for adsorption of MB using FAG

3.2.2. Effect of pH and determination of pH point of zero charge (pHpzc) of FAG

The pH is one of the most important factors controlling the adsorption of dyes onto suspended particles [53]. The effect of pH on the adsorption of MB using FAG was studied by changing initial solution pH values in the range from 2 to 12. The results are presented in Fig.6.a. It was observed after analyzing Fig.6.a that the adsorption efficiency increases from 50.45% to 98.25% as pH increases from 2.5 to 11.2. This result suggested that the activated material carried the surface net positive charge below this pH value and it possessed a net negative charge beyond this pH value [54].
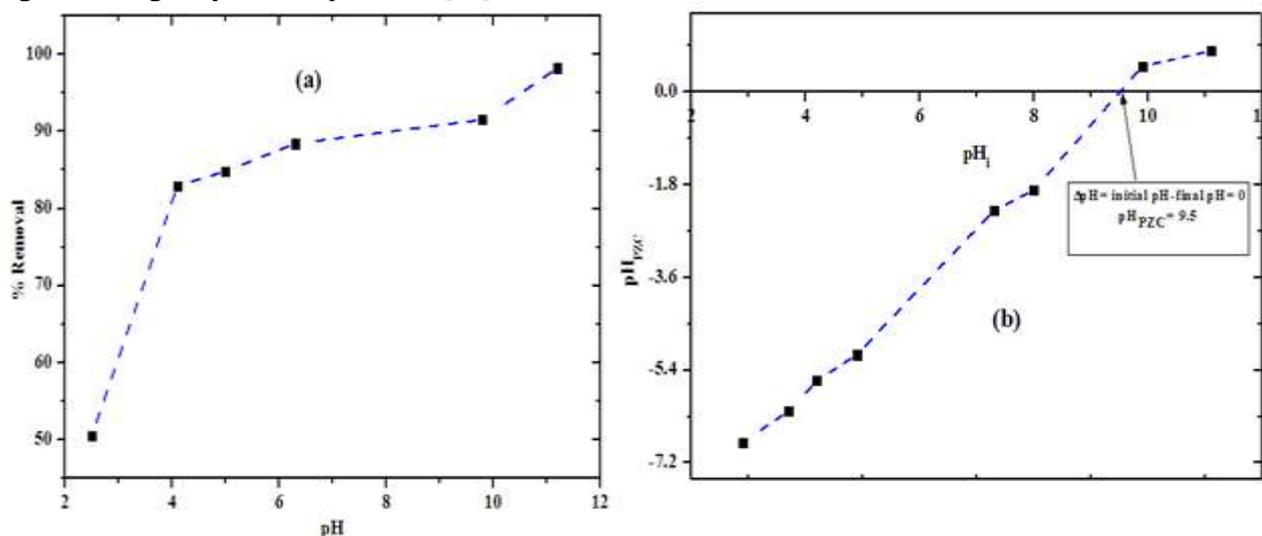

Figure 6: Effect of pH on the removal efficiency of MB on FAG (a) and Point of zero charge (pHpzc) of FAG (b)

For a better illustration of these results, it is required to determine experimentally the point of zero charge (pH_{PZC}). The point of zero charge of FAG was determined as described by the solid addition method using KNO_3 (0.01 M) solution [55, 56]. Initial pH of (0.01M) KNO_3 solutions (pH_i) was adjusted from pH 2 to 12 by adding either (0.01 M) HCl or 0.01 M (NaOH). Adsorbent dose 0.1g was added to 100 mL of 0.01 M KNO_3 solution in 100 mL conical flasks and stirred for 24 h of contact time and final pH (pH_f) of solution was measured. The difference between the initial and final pH (pH_i–pH_f) was plotted against the initial pH (pH_i) and the point where pH_i – $pH_f = 0$ was taken as the pH_{pzc}. The results obtained are shown in Fig.6.b. The pH_{pzc} of FAG determined to be 9.4. At a solution of pH<9.4 the surface becomes positively charged and pH>9.4 the FAG surface is negatively charged. The pH of the system increases and H^+ ion concentration decreases, the number of the negatively charged sites increase and the number of the positively charged sites decrease.

3.2.3. Effect of contact time

The impact of contact time on the adsorption of MB from an aqueous phase onto FAG was investigated at different time intervals in the range of 0 to 220 min. The result is shown in Fig.7. It can be seen the removal of adsorption the MB by FAG increases with the increase in time and reaches a maximum value at about 60 min for 20 and 30 mg/L, and the maximum value is observed after 120 min for 40 mg/L, after it remains constant (plateau). The amounts of dye adsorbed at equilibrium are found to be 19.39 mg/g (96.95 %), 29.87 mg/g (99.56 %) and 39.4 mg/g (98.5 %) for 20 mg/L, 30 mg/L and 40 mg/L, respectively. The result obtained in the rapid adsorption of MB significant and the time in the important parameter for adsorption the dye from aqueous phase.
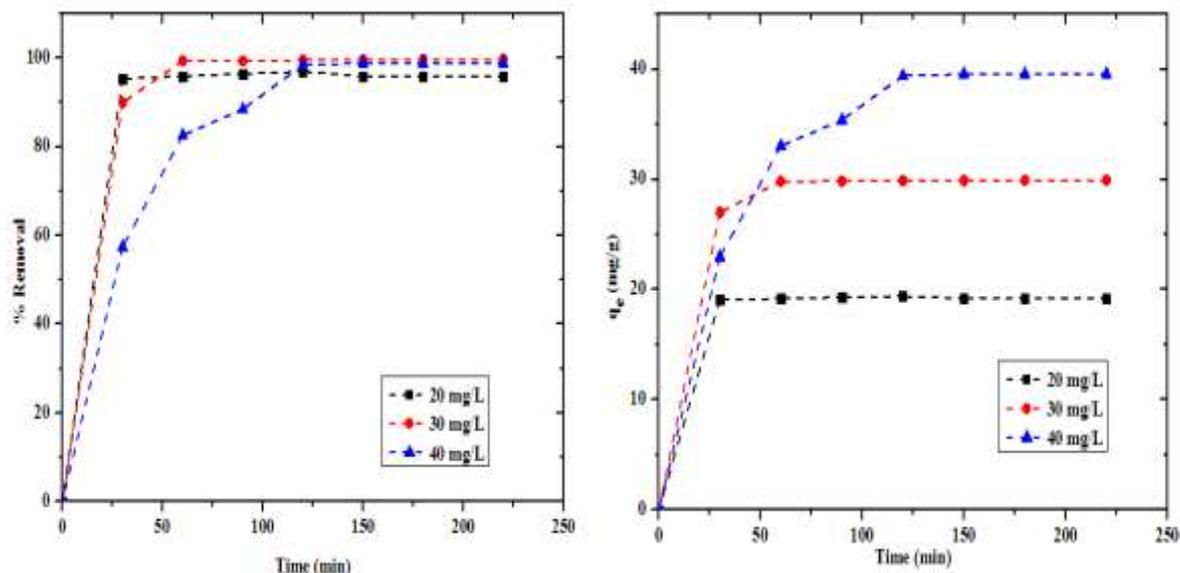

Figure 7: Effect of contact time on MB onto FAG

3.2.4. Effect of initial dye concentration

The effect of varying concentration of MB on the adsorption capacity of the MB is shown in Fig.8. As it was already expected, results obtained for the adsorption capacity at equilibrium increases from 4.89 to 36.44 mg/g, with an increase in the initial dye concentration from 5 to 60 mg/L. Following maximum adsorption, the sites of the adsorbent were filled totally with dye molecules (MB) and there are no sites available for binding [57]. Similar trend was obtained in the adsorption of MB on fly ash [58] and sulfonic acid group modified MIL-101 [59].
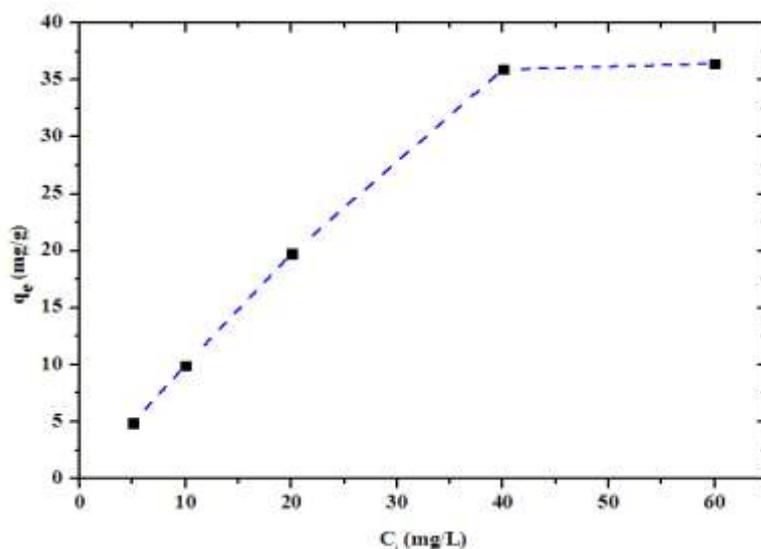

Figure 8: Effect of initial concentration on the adsorption capacity

---

3.2.5. Kinetics of adsorption

Several models have been established to describe the adsorption kinetics and the rate-limiting step of the process. They include models of pseudo-first, second-order kinetic model, model intra-particle diffusion and sorption model Weber and Morris, the relationship of Adam-Bohart Thomas, etc [60]. The adsorption kinetics data of MB using the adsorbent were analyzed with pseudo-first-order, pseudo-second-order and intraparticle diffusion kinetic models.

Pseudo-first-order kinetic model
Pseudo-first order was reported by Lagergren [61], the model is express by (4):
$$Ln(q_e - q_t) = Ln\,q_e - k_1 t \qquad (4)$$
Where q_e and q_t are the adsorption capacity at equilibrium and at time t, respectively (mg/g), k_1 is the rate constant of pseudo-first-order adsorption (1/min)

Pseudo-second-order kinetic model
The pseudo-second order model [62] is given by the equation (5):
$$\frac{t}{q_t} = \frac{1}{k_2 q_e^2} + \frac{t}{q_e} \qquad (5)$$
Where: $k_2(g \cdot mg^{-1} \cdot min^{-1})$ is the pseudo-second order rate constant, and q_t is the amount of MB adsorbed at time t (min), which was calculated from the slope and intercept of the plot t/q_t versus t.

Intraparticle diffusion process
The intraparticle diffusion equation (6) is expressed as [63]:
$$q_t = k_I t^{1/2} + I \qquad (6)$$
Where q_t is the adsorption capacity (mg/g) at time t, t is the contact time (min), k_I (mg/(g min$^{0.5}$)) and I (mg/g) are the intraparticle diffusion constants.

The experimental data of MB adsorption on FAG were simulated with three models and the results were depicted in Table 5. The correlation coefficients (R_1^2) for pseudo-first-order kinetic model are between 0.718 and 0.926, the correlation coefficients (R_2^2), for the pseudo –second- order kinetic model are between 0.99 and 1 and the correlation coefficients (R_3^2) for intraparticle diffusion model are between 0.513 and 0.993. On the basis of value R^2, the pseudo second order rate model fit best with experimental data. Also, the experimental q_e is close the calculated q_e, illustrating a strong pseudo-second-model fit the MB adsorption using the FAG, which suggested that the adsorption process is controlled by the chemisorption process. Similar kinetic results were reported for the adsorption of MB onto Spent tea leaves [64] and oil palm (Elaeis guineesis) [65].

Table 5: Kinetic parameters for adsorption of MB onto FAG

Dye C_0 mg/L	Pseudo -first-order				Pseudo-second -order			Intra-particule diffusion model		
	q_exp	q_e (mg/g)	k_1 (1/min)	R_1^2	q_e (mg/g)	k_2 (g/mg min)	R_2^2	I (mg/g)	k_id (mg/g min^0.5)	R_3^2
20 mg/L	19.19	4.007	0.022	0.718	19.23	-0.39	1	18.67	0.067	0.993
30 mg/L	29.93	7.79	0.04	0.864	30.30	0.028	0.999	26.94	0.238	0.513
40 mg/L	39.55	87	0.051	0.926	43.47	0.002	0.99	17.84	1.678	0.796

3.2.6. Isotherm models of adsorption
Adsorption isotherms were used to describe the mechanism of the interaction of MB on the adsorbent surface. Four models have been adopted in this research, namely, the Langmuir, Freundlich, D–R equilibrium and Temkin isotherm models.

Langmuir isotherm

The assumptions of Langmuir model include: the adsorption comprises the attachment of only one molecular monolayer on adsorbate surface and the ions are adsorbed on a fixed number of well-defined sites, each site can hold one ion, all sites are energetically equivalent and there is no interaction between the ions [66, 67]. The analysis of the isotherm data is important to determine the adsorption capacity of the adsorbent [68].

The form of Langmuir isotherm [69] can be given by the following equation (7):

$$\frac{C_e}{q_e} = \frac{1}{K_L q_m} + \frac{C_e}{q_m} \qquad (7)$$

Where q_e is the amount of dye adsorbed on the adsorbents at equilibrium (mg/g); C_e is the concentration of dye at equilibrium (mg/L); q_m is the maximal amount of dye ion adsorption onto the adsorbents (mg/g); and K_L is the Langmuir constant of adsorption (L/mg).

The essential characteristic of the Langmuir isotherm can be evidenced by the dimensionless constant called equilibrium parameter, R_L.

$$R_L = \frac{1}{1 + K_L C_0} \qquad (8)$$

Where b is the Langmuir constant and C_0 is the initial MB concentration, R_L values indicate the type of isotherm to be irreversible ($R_L = 0$), favorable ($0 < R_L < 1$), linear ($R_L = 1$) or unfavorable ($R_L > 1$) [70].

Freundlich isotherm

The Freundlich model is applicable to multilayer adsorption on heterogeneous surface [71]. The equation is conveniently used in the linear form as:

$$q_e = K_F C_e^{1/n} \qquad (9)$$

A linear form of this expression is:

$$Ln\, q_e = Ln\, K_F + \frac{1}{n} Ln\, C_e \qquad (10)$$

Where K_F (mg$^{(1-n)}$L^{n}g^{-1}) is the Freundlich constant and n (g/L) is the heterogeneity factor. The K_F value is related to the adsorption capacity; while 1/n value is related to the adsorption intensity.

The Dubinin–Radushkevich (D-R) isotherm

The D–R isotherm model is valid at low concentration ranges and can be used to describe adsorption on both homogeneous and heterogeneous surfaces [72].

The linear form of the isotherm can be expressed as follows [73].

$$\ln q_e = \ln(q_m) - K\varepsilon^2 \qquad (11)$$

where K is constant of the sorption energy (mol^2/kJ^2), and ε is the Polanyi potential that can be calculated from the equation:

$$\varepsilon = RT \ln(1 + \frac{1}{C_e}) \qquad (12)$$

Where R is the Universal gas constant (8.314 J.mol^{-1} K^{-1}), T (K) is the temperature and C_e (mg/L) is the equilibrium concentration of MB left in solution. q_m is the theoretical saturation capacity.

The mean energy of sorption, E (kJ/mol), is calculated by the following equation:

$$E = \frac{1}{\sqrt{(2K)}} \qquad (13)$$

The magnitude of E is useful for estimating the mechanism of the adsorption reaction. It the case of E<8 kJ/mol, physical forces may affect the adsorption. If E is in the range of 8-16 kJ /mol, adsorption is governed by ion exchange mechanism white for the value of E>16 kJ/mol, adsorption may be dominated by particle diffusion [74, 75].

Temkin model

The Temkin isotherm has been used in the following form [76].

$$q_e = B_T \ln A_T + B_T \ln C_e \qquad (14)$$

Where $B_T = R_T/b_T$, b_T is the Temkin constant related to heat of sorption (J/mol), A_T is the Temkin isotherm constant (L/g), R is the gas constant (8.314 J/mol K), and T is the absolute temperature (K).

For isotherm models: Langmuir, Freundlich, D–R isotherm and Temkin models were applied to fit the experimental data. The isotherm parameters and the values of the correlation coefficients (R^2) are summarized in Table 6. The results show that the value of R^2 obtained from Langmuir isotherm equation (0.999) was higher that from Freundlich (0.694), the D–R isotherm (0.555) and Temkin (0.866). According to the results, the correlation value R^2 for Langmuir model indicates that the adsorption MB using FAG data can be adequately modeled by the Langmuir and which indicate that adsorption of MB was made up homogenous surface and monolayer adsorption. This result is similar to other works on MB dye adsorption onto Platanus orientalis [77] and CTN/AC [78]. The maximum uptake capacity for MB removal by FAG was higher with 37.04 mg/g. The separation factor R_L is in the range of 0.05 and 0.56, showing that the adsorption of MB on FAG is favorable.

Table 6: Isotherm parameters for adsorption of MB onto FAG

Langmuir				Freundlich			Temkin			Dubinin–Radushkevich		
Q_m (mg/g)	K_L (L/mg)	R^2	Range R_L	K_F (mg$^{1-1/n}$/L$^{1/n}$g)	1/n	R^2	A_T (L/g)	B_T	R^2	Q_m (mg/g)	R^2	E (Kj/mol)
37.04	3.38	0.999	0.05-0.56	18.78	0.271	0.694	105.64	5.094	0.866	28.61	0.555	5

3.2.7. Effect of temperature and thermodynamic parameters
Effect of temperature
The effect of temperature on dye removal was studied by varying temperatures (20, 50, and 70°C). Dye reduction efficiency with temperature is shown in Fig.9. The adsorption capacity is increased slightly from 37.58 to 39.84 mg/g as the temperature increased from 20 to 70°C. Hence, the solution temperature increase leads to increase the number of active sites available to be adsorbed on the surface [79].
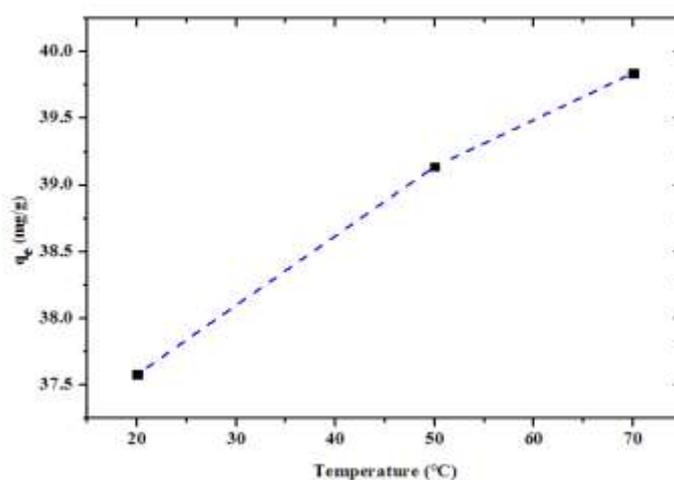

Figure 9: Effect of temperature on MB dye reduction efficiency by FAG
Thermodynamic parameters

Thermodynamic parameters are important in the design of adsorption process. It is necessary to define the change of thermodynamic parameters to predict the feasibility and mechanism of adsorption [80]. The thermodynamic parameters were determined by using following equations:

$$\Delta G^o = -RTLn\,K_d \qquad (15)$$

$$K_d = \frac{C_a}{C_e} \qquad (16)$$

$$Ln\,K_d = \frac{\Delta S^o}{R} - \frac{\Delta H^o}{RT} \qquad (17)$$

Where K_d is the distribution constant, C_a is the amount of dye adsorbed on the adsorbent of the solution at equilibrium (mol/L), C_e is the equilibrium concentration, R is the gas constant (J.mol^{-1}.K^{-1}), T is absolute temperature (K), $\Delta H°$ is the standard enthalpy, $\Delta S°$ is the standard entropy and $\Delta G°$ is the free energy.

The experimental data obtained at different temperatures are used to calculate the thermodynamic parameters. The values of $\Delta H°$, $\Delta S°$, and $\Delta G°$ for MB adsorption onto FAG are listed in Table 7. The positive values of $\Delta H°$ are indicate that the adsorption reaction is endothermic, the adsorption processes with $\Delta G°$ values in the −20 to 0 kJ mol^{-1} range correspond to spontaneous processes [81]. The $\Delta S°$ has a positive value which means increasing randomness at the solid/liquid interface, through the adsorption process of MB onto FAG reflects randomness nature of process at the solid/solution interface and the affinity of FA based geopolymer for MB adsorption [82, 83].

Table 7: Thermodynamic parameter for adsorption of MB onto FAG

adsorbent	Adsorbate	ΔH° (KJ.mol⁻¹)	ΔS° (KJ.mol⁻¹.K⁻¹)	ΔG° (KJ.mol⁻¹)		
				293K	**323K**	**343K**
FAG	**MB**	44.297	0.173	-6.681	-10.253	-15.734

3.2.8. Comparison of adsorption capacity with different adsorbent reported in literature.

Comparison of maximum monolayer adsorption capacities (based on the Langmuir adsorption isotherm) of MB using various adsorbents were reported in Table 8. The results obtained experimentally in this study are higher than the results obtained by other investigations. This clearly indicates that the FA based geopolymer can be fruitfully used as an adsorbent for cationic dye removal.

Table 8: Comparison of the maximum adsorption capacity of MB on various adsorbents

Adsorbent	Adsorption capacity (mg/g)	References
Perlite	8.79	[84]
Hyacinth root powder	8.04	[85]
Silica nano–sheets derived from Vermiculite	9.38	[86]
Natural Zeolite	23.60	[87]
Magnetic chitosan	60.4	[88]
Co₃O₄/SiO₂ nanocomposite	53.87	[89]

Fly ash	5.72	[90]
fly ash-derived zeolites	12.64	[91]
MIL-101(Cr)	22	[92]
Fe3O4@MIL-100(Fe)	49	[93]
FA based geopolymer (FAG)	37.04	This work

Conclusion

In the present study, new adsorbent has been synthesized and characterized with several techniques such as XRD, XRF, FTIR and SEM. The adsorbent was used for removal of MB from aqueous solution and the influence of several parameters, such as adsorbent ratio, solution pH, concentration of adsorbate, contact time and temperature was investigated. The experimental result indicated that the maximum adsorption of MB dye by FAG occurred at a basic environment. Kinetic studies reveal that FAG can remove MB quickly, within 120 min and the adsorption results indicated that the adsorption kinetics followed a pseudo-second-order kinetics model. The adsorption Langmuir model producing the best results, which indicated that it is monolayer adsorption of MB. The maximum adsorption capacity for MB by the used FAG is 37.04 mg/g. Temperature shows a small influence on the adsorption of MB onto FAG. Thermodynamic parameters calculations confirm that the adsorption of MB onto FAG is a spontaneous, favorable and endothermic process. In the view of these results, it can be concluded that the new adsorbent synthesized by FA and alkaline solution was the preferable choice as excellent adsorbent for the reduction of MB from aqueous solution.

References
1. S. Barreca, S. Orecchio, A. Pace, *Appl. Clay Sci*. 99 (2014) 220–228.
2. M. Hwang, K. Chen, *J. Appl. Polym. Sc*. 49 (1993) 975–989.
3. S. Nawar, H. Doma, *Sci. Total Environ*. 79 (1989) 271–279.
4. M. A. M. Salleh, D. K. Mahmoud, W. A. Karim, A. Idris, *Desalination*. 280 (2011) 1–13.
5. M.H. El-Naas, S. A. Al-Muhtaseb, S. J. Makhout, *Hazard. Mater*. 164 (2009) 720–725.
6. C. Tocchi, E. Federici, L. Fidati, R. Manzi, V. Vincigurerra, M. Petruccioli, *Water Res*. 46 (2012) 3334–3344.
7. Y. Zhang, C. Causserand, P. Aimar, J. P. Cravedi, *Water Res*. 40 (2006) 3793–3799.
8. A. Dbrowski, Z. Hubicki, P. Podkocielny, E. Robens, *Chemosphere*. 56 (2) (2004) 91–106.
9. D.J. Ennigrou, L. Gzara, M.R. Ben Romdhane, Dhahbi, *Desalination*. 246 (1-3) (2009) 363–369.
10. B. Mondal, V.C. Srivastava, J.P. Kushawaha, R. Bhatnagar, S. Singh, I.D. Mall, *Sep. Purif. Technol*. 109 (2013) 135–143.
11. A.K. Verma, R.R. Dash, P. Brunia, *J. Environ. Manage*. 93 (2012) 154–168.
12. I. Hachoumi, I. El Ouahabi, R. Slimani, B. Cagnon, M. El Haddad, El Antri, S. Lazar, *J. Mater. Environ. Sci*. 8 (4) (2017) 1448–1459.
13. G. Vijayakumar, R. Tamilarasan, M. Dharmendirakumar, *J. Mater. Environ. Sci*. 3 (1) (2012) 157–170.
14. N. Barka, S. Qourzal, A. Assabbane, A. Nounah, Y. Ait-Ichou, *J. Environ. Sci*. 20 (2008) 1268–1272.
15. V.S. Mane, I.D. Mall, V.C. Srivastava , *J. Environ. Manage*. 84 (4) (2007) 390–400.
16. P. Janos, H., M. Ryznarova, *Water Res*. 37 (20) (2003) 4938–4944.
17. Z. Eren, F.N. Acar, *J. Hazard. Mater*. 143 (1) (2007) 226–232.
18. S. Wang, Z.H. Zhu, *J. Hazard. Mater*. 126 (2005) 91–95.
19. M. Rachakornkij, S. Ruangchuay, S. Teachakulwiroj, *J. Sci. Techno*. 26 (2004)13–24.
20. I. Uzun, *Dyes Pigm*. 70 (2006) 76–83.
21. G. McKay, *AIChE J*. (1984) 30–692.
22. N. Barka, A. Assabbane, A. Nounah, L. Laanab, Y. Aît-Ichou, *Desalination*. 235 (2009) 264–275.
23. T. Thiebault, R. Guégan, M. Boussafir, *J. Colloid. Interf. Sci*. 453 (2015) 1–8.
24. B.H. Hameed, M.I. El-Khaiary, *J. Hazard. Mater*. 157 (2008) 344–351.
25. T.W. Cheng, M.L. Lee, M.S. Ko, T.H. Ueng, S.F. Yang, *Appl. Clay Sci*. 56 (2012) 90–96.
26. Y. Zhang, L. Liu, *Particuology*. 11 (2013) 353–358.

27. D.J. Ennigrou, L. Gzara, M.R. Ben Romdhane, M. Dhahbi, *Desalination*. 246 (1-3) (2009) 363.

28. J. Davidovits, Proceedings of PACTEC'79, Society of Plastic Engineers. Brookfield Center, USA, (1979) 15–154.

29. J. Davidovits, *U.S.* Pat. No. 3, 950, 470, (1976).

30. J. Davidovits, Proceedings of the 2 nd International Conference on Geopolymere, Saint-Quentin, France 9–40. June 30-July 2, 1999.

31. J. Davidovits, *J. Therm. Anal.* 37 (1991) 1633–1656.

32. Y. Zhang, L. Liu, *Particuology*. 11 (2013) 353– 358.

33. M.S. Al-Harahsheh, K. Al Zboon, L. Al-Makhadmeh, M. Hararah, M. Mahasneh, *J. Environ. Chem. Eng.* (2015).

34. L. Li, S. Wang, Z. Zhu, *J. Colloid Interface Sci.* 300 (2006) 52–59.

35. N. Koshy, D.N. Singh, *J. Environ. Chem. Eng.* 4 (2) (2016) 1460–1472.

36. H. Xu, J.S.J. Van Deventer, *Int. J. Miner. Process.* 59 (2000) 247–266.

37. W.K.W. Lee, J.S. Deventer, *J. Colloids Surf. A.* 211 (2002) 49–66.

38. S. Ryu, Y. Lee, B.K.T. Koh, Y.S. Chung, *Constr. Build. Mater.* 47 (2013) 409–418.

39. J. Davidovits, 30 years of successes and failures in geopolymer applications, Market trends and potential breakthroughs. In: Geopolymer Conference. Saint-Quentin (France), Melbourne (Australia): Geopolymer Institute. (2002).

40. M. Y. J. Liu, U. J. Alengaram, M. Santhanam, M.Z. Jumaat, K.H. Mo, *Constr. Build. Mater.* 120 (2016) 112–122.

41. M. Criado, A. Palomo, A. Fernandez-Jimenez, *Fuel.* 84 (2005) 2048–2054.

42. E. Alvarez-Ayuso, X. Querol, F. Plana, A. Alastuey, N. Moreno, M. Izquierdo, O. Font, T. Moreno, S. Diez, E. Vazquez, l. Barra, *J. Hazard. Mater.* 154 (2008) 175–183.

43. S. Kumar, F. Kristaly, G. Mucsi, *Adv. Powder Technol.* 26 (2015) 24–30.

44. A. Gok, M. Omastova, J. Proke, *Eur. Polym. J.* 43 (2007) 2471–2480.

45. S.K. Nath, S. Maitra, S. Mukherjee, Sanjay Kumar, *Constr. Build. Mater.* 111 (2016) 758–765.

46. G. Kovalchuk, A. Fernandez-Jimenez, A. Palomo, *Fuel*. 86 (2007) 315–322.

47. B.T. Poe, P.F. McMillan, C.A. Angell, R.K. Sato, *Chem. Geol.* 96 (3–4) (1992) 333–349.

48. I. Kara, D. Yilmazer, T.A. Akar, *Appl. Clay Sci*. 139 (2017) 54–63.

49. W.K.W. Lee, J.S. Van Deventer, *J. Colloid Surf. A* 211 (2–3) (2002) 115–126.

50. J.C. Swanepoel, C.A. Strydom, *Appl. Geochem.* 17 (8) (2002) 1143–1148.

51. S. Kumar, F. Kristaly, G. Mucsi, *Adv. Powder Technol.* 26 (2015) 24–30.

52. A.T. Kah, M. Norhashimah, T. Tjoon, T. Ismail Norli, P. Panneerselvam, *APCBEE Procedia.* 1 (2012) 83–89.

53. N. Barka, S. Qourzal, A. Assabbane, A. Nounah, Y. Ait-Ichou, *J. Saudi Chem. Soc.* 15 (2011) 263–267.

54. R. Pawar, R. Lalhmunsiama, H.C. Bajaj, Seung-Mok Lee, *J. Ind. Eng. Chem.* 34 (2016), 213–223.

55. I.D. Mall, V.C. Srivastava, G.V.A. Kumar, I.M. Mishra, *Colloids Surf. A: Physicochem. Eng. Aspects.* 278 (2006) 175–187.

56. S.M. Oliveira Brito, H.M.C. Andrade, L.F. Soares, R.P. de Azevedo, *J. Hazard. Mater.* 174 (2010) 84–92.

57. V.P. Mahida, M. P. Patel, *Arab. J. Chem.* http://dx.doi.org/10.1016/j.arabjc.2014.05.016.

58. V.V. Basava Rao, S. Ram Mohan Rao, *Chem. Eng. J.,* 116 (2006) 77–84.

59. X.P. Luo, S.Y. Fu, M. DuY, J.Z. Guo, B. Li, *Microporous Mesoporous Mater.* (2016), doi:10.1016/j.micromeso.2016.09.032.

60. J. Febrianto, A.N. Kosasih, J. Sunarso, Y. Ju, N. Indraswati, S. Ismadji, *J. Hazard. Mater.* 162 (2009) 616–645.

61. S. K. Lagergren, *Sven. Ventensk. Akad. Hand.* 24 (1898) 1–39.

62. Y.S. Ho, G. McKay, *Process Biochem.* 34 (1999) 451–465.

63. T. Furusawa, J.M. Smith, *Aiche J.* 20 (1974) 88-93.

64. B.H. Hameed, *J. Hazard. Mater.* 161 (2–3) (2009) 753–9.

65. H.D. Setiabudi, R. Jusoh, S. Suhaimi, S.F. Masrur, *J. Taiwan Inst. Chem. Eng.* 63 (2016) 363–370.

66. V.K. Gupta, I. Ali, *J. Colloid Interface Sci.* 271 (2) (2004) 321–328.

67. N. Ahalya, R.D. Kanamadi, T.V. Ramachandra, *Electron. J. Biotechnol.* 8 (2005) 258–264.

68. R. M. Ali, H.A. Hamada, M. M. Hussein, G. F. Malash, *Ecol Eng*. 91 (2016) 317–332.

69. I. Langmuir, *J. Am. Chem. Soc.* 40 (9) (1918) 1361–1403.

70. R.A. Shawabkeh, M.F. Tutunji, *Appl. Clay Sci*. 24 (2003) 111–120.

71. K.Y. Foo, B.H. Hameed, *Chem. Eng. J.* 156 (2010) 2–10.

72. T. Shahwan, H.N. Erten, *J. Radioanal. Nucl. Chem.* 260 (2004) 43–48.
73. M.M. Dubinin, L.V. Radushkevich, *Proc. Acad. Sci. USSR Phys., Chem. Sect.* 55 (1947) 331–337.
74. A.S. Ozcan, B. Erdem, A. Ozcan, *Colloids Surf. A: Physicochem. Eng. Aspects*. 266 (2005) 73–81.
75. A. Özcan, E.M. Öncü, A.S. Özcan, *Colloids Surf. A.* (1-3) 277 (2006) 90–97.
76. M. I. Temkin, *Zh. Fiz. Chim.* 15 (1941) 296–332.
77. M. Peydayesh, A. Rahbar-Kelishami*, J. Ind. Eng. Chem.* (2014).
78. H. Karaer, Ismet Kaya, *Microporous Mesoporous Mater.* 232 (2016) 26-38.
79. K. Krishnan, T.S. Anirudhan, *Indian J. Chem. Technol.* 9 (2002) 32–40.
80. H. Karaer, I. Kaya, *Microporous Mesoporous Mater.* (2016).
81. Z. Bouberka, A. Khenifi, N. Benderdouche, Z. Derriche, *J. Hazard. Mater.* 133 (1-3) (2006) 154-61.
82. D. Pathania, S. Sharma, P. Singh, *Arab. J. Chem.,* (2013). http://dx.doi.org/ 360 10.1016/j.arabjc.2013.04.021
83. I. Mobasherpour, E. Salahi, M. Ebrahimi, *J. Saudi Chem. Soc.* 18(6) (2014) 792–801.
84. M. Dogan, M. Alkan, A. Türkyilmaz, Y. Özdemir, *J. Hazard. Mater.* 109 (1-3) (2004) 141–148.
85. M. Soni, A.K. Sharma, J.K. Srivastava, S. Yadav, *Int. J. Chem. Sci. Appl.* 3 (2012) 338–345.
86. M. F. Zhao, Z. B. Tang, P. Liu, *J. Hazard. Mater.* 158 (2008) 43–51.
87. F. Jafari-zare, A. Habibi-yangjeh, *Chin. J. Chem.* 28 (2010) 349–356.
88. M. Auta, B.H. Hameed, *Chem. Eng. J*. 237 (2014) 352–361.
89. H.H. Abdel Ghafar, G.A.M. Ali, O.A. Fouad, S.A. Makhlouf, *Desalin. Water Treat.* 53 (2013) 2980– 2989.
90. K.V. Kumar, V. Ramamurthi, S. Sivanesan, *J. Colloid. Interf. Sci.* 284 (2005) 14–21.
91. C.D. Woolard, J. Strong, C.R. Erasmus, *Appl. Geochem.* 17 (9) (2002) 1159–1164.
92. T. Shen, J. Luo, S. Zhang, X. Luo, *J. Environ. Chem. Eng.* 3 (2015) 1372–1383.
93. Y. Shao, L. Zhou, C. Bao, J. Ma, M. Liu, F. Wang, *Chem. Eng. J.* 283 (2016) 1127–1136.

(2018) ; http://www.jmaterenvironsci.com